Shifting patterns of lake color phenology in over 26,000 US lakes

2   **Simon N. Topp*[1], Tamlin M. Pavelsky[1], Hilary A. Dugan[2], Xiao Yang[1], John Gardner[1,3], Matthew R.V. Ross[4]**

4   [1] Department of Geological Sciences, University of North Carolina at Chapel Hill

[2] Center for Limnology, University of Wisconsin-Madison

6   [3] Department of Geology and Environmental Science, University of Pittsburgh

[4] Department of Ecosystem Science and Sustainability, Colorado State University

8   *Corresponding author: Simon N. Topp (sntopp@live.unc.edu)

Key Points:

10   • Summer lake color phenology can be generalized into five distinct seasonal patterns of greening and blueing events

12   • Since the mid-1990s, the number of lakes with color patterns corresponding to eutrophic waterbodies has been increasing

14   • We observe these patterns using a new U.S. lake remote sensing dataset that contains over 22 million lake observations

16 **Abstract**

Lakes are often defined by seasonal cycles. The seasonal timing, or phenology, of many lake
18 processes, such as primary productivity, are changing in response to human activities. However,
long-term records exist for few lakes, and extrapolating patterns observed in these lakes to entire
20 landscapes is exceedingly difficult using the limited number of in situ observations that are
available. Limited landscape level observations means we do not know how common shifts in
22 lake phenology are at macroscales. Here, we use a new remote sensing dataset, LimnoSat-US, to
analyze U.S. summer lake color phenology between 1984 and 2020 across more than 26,000
24 lakes. Our results show that summer lake color seasonality can be generalized into five distinct
phenology groups that follow well-known patterns of phytoplankton succession. The frequency
26 with which lakes transition from one phenology group to another is tied to lake and landscape
level characteristics. Lakes with high discharge and low variation in their seasonal extent are
28 generally more stable while lakes in areas with high interannual variations in climate and
catchment population density show less stability. Our research reveals previously unexamined
30 spatiotemporal patterns in lake seasonality and demonstrates the utility of LimnoSat-US, which,
with over 22 million remote sensing observations of lakes, creates novel opportunities to
32 systematically examine changing lotic ecosystems at a national scale.

Plain Language Summary

34 Lakes naturally have seasonal cycles that result in yearly peaks in algal growth. The size and
timing of these peak periods depends on the amount of nutrients available and the timing of key
36 events such as freezing and thawing. Bluer lakes with little algae typically have one peak in the
spring, while greener, high algae lakes can have multiple peaks or longer duration peaks that
38 span the summer months. As such, color is a useful tool for measuring the characteristics of lake
ecosystems. Here, we look at how these seasonal cycles changed in over 26,000 lakes across the
40 United States between 1984 and 2020. We find that while some lakes are getting bluer,
particularly in the Pacific Northwest, there has also been an increase in the number of lakes that
42 show seasonal cycles associated with high algae waterbodies. Lakes at high elevations and in
catchments with large year-to-year fluctuations in temperature and population density are most
44 prone to changes in seasonal cycles over time.

46 **1 Introduction**

Lakes are critical freshwater resources that are highly sensitive to stressors such as climate
48 change (Woolway et al., 2020) and altered land use (Martinuzzi et al., 2014). Globally, these
stressors are shortening the duration of ice cover (Sharma et al., 2019), increasing rates of lake
50 carbon burial (Heathcote & Downing, 2012), increasing evaporative water loss (Wang et al.,
2018), warming surface waters (O'Reilly et al., 2015), and changing mixing regimes (Maberly et
52 al., 2020; Woolway & Merchant, 2019), all of which influence lake productivity and ecological
state. These changes manifest themselves in the seasonality of lake processes. Just like a
54 deciduous forest that comes to life in the spring, inland water bodies are characterized by a
predictable seasonal succession of biological processes (Sommer et al., 2012). In the spring,
56 many lakes experience a diatom bloom, followed by a 'clear-water' phase where zooplankton
rapidly devour the newly plentiful phytoplankton (Matsuzaki et al., 2020). Summer algal
58 biomass is constrained by nutrient availability, with nutrient-rich eutrophic lakes experiencing
near-constant summer phytoplankton blooms, and nutrient-poor oligotrophic lakes experiencing

60 relatively clear waters (Sommer et al., 1986). The difference between these states is visible to the naked eye, as the predominant color of a lake lies along a spectrum of blue (oligotrophic) to
62 green (eutrophic); or as dissolved carbon concentrations increase, brown (dystrophic) (Webster et al., 2008).

64 The color of a lake reveals a lot about lake productivity and ecological state. A green lake will have a greater abundance of phytoplankton and a higher rate of carbon burial than a blue lake
66 (Heathcote & Downing, 2012). Browning or greening of oligotrophic lakes may result in oxygen depletion and anoxic conditions (Knoll et al., 2018; Müller et al., 2012), which impacts nutrient
68 cycling. Shifts in the magnitude and timing of annual color changes are indicators of short-term external (weather, nutrient, and carbon loading) and internal (biology) factors and/or long-term
70 climate, watershed, and food web changes. These changes are not confined to single lakes, with landscape-level drivers impacting the color regimes of entire regions. For instance, shortened ice
72 cover durations (Sharma et al., 2019) are shifting the spring-phytoplankton bloom earlier (Winder & Schindler, 2004), increases in dissolved organic carbon are browning lakes (Monteith
74 et al., 2007; Roulet & Moore, 2006), and invasive zebra mussels are increasing water clarity (Binding et al., 2007), all at regional scales.

76 For a single lake, observing the annual pattern of lake color provides insight into the local ecosystem. At larger scales, simultaneously observing the annual patterns of many lakes provides
78 evidence of the impacts of climate and land-use change and is critical in understanding the role of inland waters in carbon production and sequestration. Remote sensing enables this macroscale
80 freshwater analysis because it captures a wide range of hydrologic conditions (e.g. Allen et al., 2020) with regular sampling intervals and global coverage. The Landsat series of satellites
82 specifically provides over three decades of observations and can be used to accurately estimate water quality parameters such as chl-a and algal blooms (Cao et al., 2020; Dekker & Peters,
84 1993; Ho et al., 2019), colored dissolved organic matter (CDOM) (Griffin et al., 2018; Olmanson et al., 2020), suspended sediments (Dekker et al., 2001; Ritchie & Cooper, 1988), water clarity
86 (McCullough et al., 2013; Olmanson et al., 2008), and primary productivity (Kuhn et al., 2020). To infer water quality, these studies build models based on relationships between optically active
88 constituent concentrations and their impact on water surface reflectance. These efforts are becoming increasingly accessible due to emerging datasets that match satellite observations with
90 field measurements of water quality parameters for model training and development (Dethier et al., 2020; Ross et al., 2019; Spyrakos et al., 2020), as well as online processing and data storage
92 platforms such as Google Earth Engine (Gorelick et al., 2017).

   Here, we present a 36 year analysis of U.S. lake color phenology using LimnoSat-US, a new
94 analysis-ready remote sensing dataset for inland waters. LimnoSat-US contains all cloud-free Landsat observations of U.S. lakes larger than 0.1 km^2 between 1984-2020. As either a stand-
96 alone resource, or when combined with existing datasets such as AquaSat (Ross et al., 2019) and RiverSR (Gardner et al., 2020), LimnoSat-US provides opportunities for novel analyses of
98 remotely sensed, macroscale patterns in U.S. freshwater resources. Through this initial application of LimnoSat-US, we attempt to identify the dominant phenology patterns in U.S.
100 lakes, how those patterns have changed over time, and what lake and landscape level characteristics control the stability of a given lake's seasonal cycle.

102 **2 Materials and Methods**

   2.1 Database Development

104 We constructed the LimnoSat-US database (Topp et al., 2020) by extracting USGS Tier 1
     Landsat Surface Reflectance (T1-SR) (Rs) values over 56,792 lakes (HydroLAKES, Messager et
106 al., 2016) across >328,000 scenes from Landsat 5 Thematic Mapper (TM), Landsat 7 Enhanced
     Thematic Mapper (ETM+), and Landsat 8 Optical Land Imager (OLI) sensors dating back to
108 1984. These observations include lakes throughout the conterminous United States and those
     directly adjacent to its border. While these surface reflectance products were originally
110 developed for terrestrial applications, a growing body of research shows that they can be used to
     accurately estimate inland water quality parameters and perform on par with water-specific
112 atmospheric correction algorithms (Griffin et al., 2018; C. Kuhn et al., 2019; Olmanson et al.,
     2020). Within the T1-SR catalogues, Landsat 5 and Landsat 7 imagery are atmospherically
114 corrected using the Landsat Ecosystem Disturbance Adaptive Processing System (LEDAPS)
     (Masek et al., 2006) while Landsat 8 images are corrected using the Landsat Surface Reflectance
116 Code (LaSRC) (Dwyer et al., 2018; Vermote et al., 2016). We extracted reflectance values using
     an optimized workflow within Google Earth Engine (Gorelick et al., 2017) comprised of three
118 key steps: 1) the calculation of the 'deepest' point (Chebyshev Center, Shen et al., 2015) for each
     lake within HydroLAKES; 2) water masking and extracting summary optical properties
120 surrounding each deepest point; and 3) standardization of reflectance values across sensors
     (Figure S1).

122 Previous studies have used the centroids of lake polygons as representative locations for deep-
     water lake conditions (e.g. Soranno et al., 2017). However, there is no guarantee that the location
124 of the centroid lies within the area defined by the polygon, nor that the centroid is necessarily the
     furthest point from the lake shore (Figure S2). Pulling satellite reflectance values from centroids
126 that fall within shallow littoral waters increases the likelihood of influence from the bed and
     nearshore land pixels (Volpe et al., 2011). To remedy this problem, we instead used the
128 Chebyshev Center, or "deepest point", of a lake polygon. The Chebyshev Center is defined as the
     center of the largest circle that can fit entirely within a given polygon's boundary (Shen et al.,
130 2015). We estimated the deepest point for each lake in Google Earth Engine (Gorelick et al.,
     2017) by identifying the location of the pixel that is furthest away from the lake shoreline (Yang,
132 2020)

     Pixels within 120 meters of the deepest point were classified using the USGS Dynamic Surface
134 Water Extent algorithm (DSWE) (Jones, 2015, 2019) and the USGS Landsat Tier 1 Surface
     Reflectance pixelQA band as derived by the CFMask cloud detection algorithm (Zhu et al.,
136 2015). Observations were removed if any clouds, cloud shadow, snow, or ice were detected
     within the 120 meter buffer around the deepest point. Median values for all bands were
138 subsequently calculated from high confidence water pixels as defined by DSWE (observations
     with less than 9 pixels of high confidence water were removed). While conservative, we assume
140 the process of taking the median of only high confidence water pixels within 120 meters of the
     deepest point limits the impacts of adjacency effects, bottom reflectance, and possible noise due
142 to wind-induced sun glint and surface or benthic macrophytes that may be prevalent in shallower
     waters. Final values are based solely on high confidence water pixels, but total counts of high
144 confidence water pixels and partial surface water (vegetated) pixels were calculated in order to
     provide an indication of potential mixed pixels and/or noise in the final reflectance values. To
146 address sensor variation and differences in atmospheric correction procedures, bands for each
     sensor were standardized following Gardner et al. (2020). Specifically, reflectance values were
148 filtered to coincident time periods (1999-2011 for Landsat 5 and 7; 2012-2020 for Landsat 7 and
     8) and Landsat 5 and 8 were standardized to Landsat 7 values through a second order polynomial

150 regression of the 1-99th percentile values of each sensor (Figure S3). Similar efforts focused on terrestrial applications have shown that statistical sensor correction can effectively improve
152 multi-sensor continuity (Roy et al., 2016).

This process was optimized by iterating over Landsat WRS tiles and applying all necessary
154 calculations in a single pass over each image/lake center. This approach dramatically speeds up computation on the Earth Engine servers by reducing the number of distinct image stacks
156 generated and reducing the number of passes necessary to extract summary metrics from each lake within a given image. These performance operations become increasingly important as the
158 size of analysis increases. While it varies with Earth Engine traffic, the optimized pipeline presented here decreases computation time for the >328,000 images in the analysis from
160 approximately 30 days to 5 days for the contiguous U.S. when compared to pipelines using multiple passes and/or iterating by lake rather than WRS tile.

162   2.2 Estimating Lake Color

Water color, as perceived by the human eye, is an intuitive measure of lake water properties.
164 Color can be directly measured by any optical imager with bands in the visible spectrum and does not require knowledge of the inherent optical properties of water (Giardino et al., 2019;
166 Woerd & Wernand, 2015). We quantified lake color as the dominant wavelength (λd) within the human visible spectrum by transforming surface reflectance into the chromaticity colorspace
168 following Wang et al. (2015). Tristimulus values (X,Y,Z, Equation 1) were calculated from surface reflectance values (red, green, blue) and then converted into chromaticity coordinates (x,
170 y, z, Equation 2).

$$X = 2.7689R + 1.7517G + 1.1302B$$
172
$$Y = 1.0000R + 4.5907G + 0.0601B$$

$$Z = 0.0565G + 5.5943B$$

174   (Equation 1)

$$x = \frac{X}{X+Y+Z} \qquad y = \frac{Y}{X+Y+Z} \qquad z = \frac{Z}{X+Y+Z}$$

176   (Equation 2)

178 Using these coordinates, the hue angle is calculated (Equation 3) and converted into λd using the International Commission on Illumination (CIE) look-up tables.

180

$$\alpha = \left(arctan2 \frac{x-0.33}{y-0.33}\right) \frac{180}{\pi}$$

182   (Equation 3)

In addition to dominant wavelength, which has known non-linearities in its distribution, we also
184 calculated lake color within the Forel-Ule Color Index (FUI) space (Wang et al., 2015). The FUI is a discrete set of 21 colors that were developed specifically to identify water-color typologies
186 (Barysheva, 1987). FUI values can be accurately calculated from multispectral imagery (Van der Woerd & Wernand, 2018; Wang et al., 2020) using either dominant wavelength or hue angle.
188 Here, we use FUI values to more precisely show how we perceive various dominant

190 wavelengths, the water-color typologies different wavelengths are associated with, and to assist in the visualization of color distributions.

2.2 Seasonal lake color phenology

192 The development of the LimnoSat-US database provides novel opportunities for examining macrosystem patterns in U.S. lake dynamics. Clustering analysis is one common approach for
194 extracting patterns from time series datasets that have no *a priori* assumptions about group membership (Warren Liao, 2005) with successful applications in fields such as hydrology
196 (Brunner et al., 2020; Savoy et al., 2019), ecology (Xue et al., 2014; Zhang & Hepner, 2017), and biogeochemistry (Byrnes et al., 2020). The overall goal of clustering analysis is to partition
198 group membership based on within-group similarity and between-group dissimilarity. Here, we apply clustering analysis to time series of lake color to better understand the drivers of variation
200 in lake seasonality over the past 36 years.

Lake color observations generated from the LimnoSat-US database were filtered to those
202 between May and October to remove missing data caused by snow and ice. Observations were broken into 6 distinct periods - (1984, 1990], (1990, 1996], (1996, 2002], (2002, 2008], (2008,
204 2014], (2014, 2020] - and were filtered to those with at least three observations per month per period, resulting in 26,607 lakes with enough data to calculate periodic seasonality for the
206 analyses. Within each period, lake color phenology was calculated for both raw dominant wavelength and lake/period z-normalized dominant wavelength using a Nadaraya–Watson kernel
208 regression (Nadaraya, 1964; Watson, 1964) implemented with the kmsooth function from the stats package in R (RCore Team, 2019). Application of the kernel regression allowed for the
210 calculation of a weekly color value based on a gaussian weighted average of all observations within a window of 21 days from the point calculated. Extreme outliers (>4 standard deviations
212 from the lake/period mean) were removed prior to the kernel regression for each series. The resulting time series consist of weekly estimates of lake color from May to October for each lake
214 for each period (Figure 1).

Normalization of the time series is critical for accurately clustering lake phenologies using the
216 dynamic time warping (DTW) method described below (Keogh & Kasetty, 2003; Mueen & Keogh, 2016). However, by standardizing the variance across time series, we artificially impose
218 equal seasonal variation between lakes/periods that are relatively monotonic (i.e. aseasonal) and those that show true seasonality in the phenology of their color. Examination of the mean and
220 standard deviation of dominant wavelength for the non-normalized time series shows that this is particularly problematic for end member lakes on either end of the color spectrum that show very
222 little seasonal variation (σ < 5 nm, Figure S4). This can be seen in Figure 1, where oligotrophic Crater Lake shows minimal seasonality when compared to known eutrophic waterbodies (Lake
224 Mendota and Lake Okeechobee). To address this issue while still following best practices of normalization for clustering analysis, those lakes/periods with a dominant wavelength standard
226 deviation of less than 5 nm were classified *a priori* as aseasonal. This threshold guarantees that seasonal variation within any remaining time series is at least ~10 nm around the mean color
228 while effectively classifying aseasonal, monotonic, and end-member lakes as their own grouping.

This process resulted in 109,643 individual time series available for cluster analysis and an
230 additional 46,759 classified *a priori* as aseasonal. These time series were clustered using dynamic time warping (DTW) (Sakoa and Chiba, 1978) within a partitional clustering
232 framework with barycenter averaging (Sarda-Espinosa et al., 2019). Dynamic time warping

234 allows points within two time series to be compared within a user-defined window as opposed to using a one-to-one comparison found in traditional metrics like Euclidean distance. This elasticity reduces the impacts of noise, minor temporal shifts, and outliers, making it ideal for

236 ecological systems with natural interannual variations (Savoy et al., 2019; Xue et al., 2014; Zhang & Hepner, 2017). The final number of clusters was determined by comparing the Davies-

238 Bouldin (Davies & Bouldin, 1979) and Modified Davies-Bouldin (Kim & Ramakrishna, 2005) cluster validity indexes (CVI) across iterations ranging from 2 to 8 clusters. The Davies-Bouldin

240 and Modified Davies Bouldin were chosen because of their computational efficiency and strong performance when compared to other common CVIs (Arbelaitz et al., 2013).

242
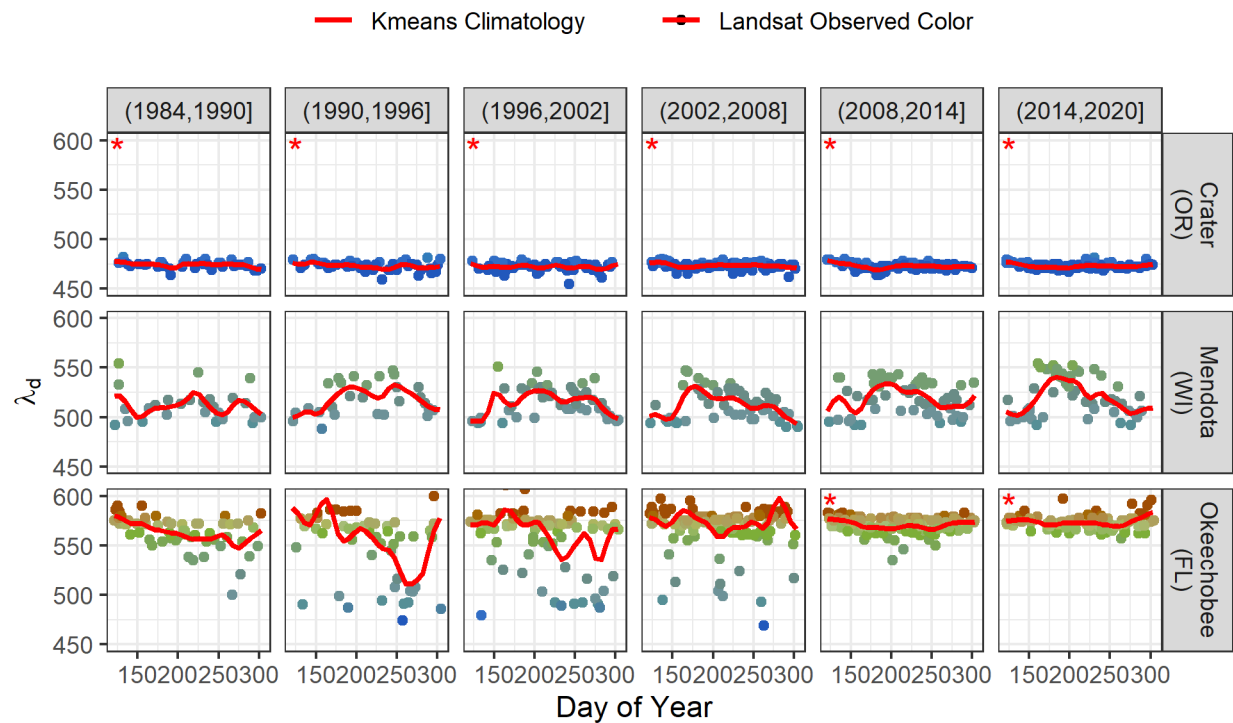
Figure 1: Examples of the calculated seasonal phenologies for three well studied lakes of

244 different trophic states. Phenologies are composed of one observation per 7 days calculated by taking a gaussian weighted average of all points +/- 21 days from each calculated point.

246 Lakes/periods marked by an asterisk were classified as aseasonal and placed in the *a priori* aseasonal cluster.

248 One important validation of clustering analysis is how sensitive final clusters are to sample variations in their input, the idea being that stable, or 'universal', clusters will emerge across

250 differing sampling schemes (Jain & Moreau, 1987). Here, we addressed issues of cluster stability using the Jaccard Similarity Index across 100 iterations of bootstrap sampling of our input time

252 series. At each iteration, the original input time series were sampled with replacement, clustered, and the resulting clustering algorithm used to predict groupings for the original data. The Jaccard

254 Similarity Index was then calculated based on how similar each new cluster was to the corresponding original cluster. The index ranges from 0 to 1, indicating that clusters share all or

256 no members, with values greater than 0.5 generally indicating cluster stability and representativeness of true patterns within the data (Savoy et al., 2019). Significant differences in

258   the distribution characteristics of the final clusters were identified using the non-parametric Kruskall Wallace Analysis of Variance on Ranks (Hollander & Wolfe, 1973) followed by
260   Dunn's Test with a Bonferroni p-value correction (Dunn, 1961).

       Finally, we examined the spatial autocorrelation of clusters and the overall stability of individual
262   lake phenologies. Spatial autocorrelation was measured by randomly sampling 30% of the lakes, assigning them their most common cluster, and calculating the proportion of same cluster lakes
264   versus different cluster lakes within 50 km windows moving outward from each lake in the subsample. Lake phenology stability was calculated by examining the number of times a given
266   lake shifted between clusters throughout the 6 periods of study. Lakes were categorized on a scale from 0 (stable) to 5 (unstable) based on the total number of cluster transitions they made
268   between 1984 and 2020. Lake and landscape level factors from HydroLAKES (Messager et al., 2016) and the Global Lake Area, Climate, and Population database (Meyer et al., 2020) were
270   then used to assess lake characteristics that influence the stability of a lake's seasonal phenology over time. Variables that potentially influence stability were identified through linear regression
272   of lake stability (0-5) on the median value of the lake/climate attribute within each stability class. Those attributes with a coefficient p-value of less than 0.05 were further examined as correlates
274   with lake stability.

3 Results

276   The final LimnoSat-US database includes reflectance values spanning 36 years for 56,792 lakes across > 328,000 Landsat scenes. After initial quality control measures, the database contains
278   over 22 million individual lake observations with an average of 393 +/- 233 (mean +/- standard deviation) observations per lake over the entire study period. While observations date back to
280   1984, the total number for any given year approximately doubles with the launch of Landsat 7 in 1999 (Figure 2).
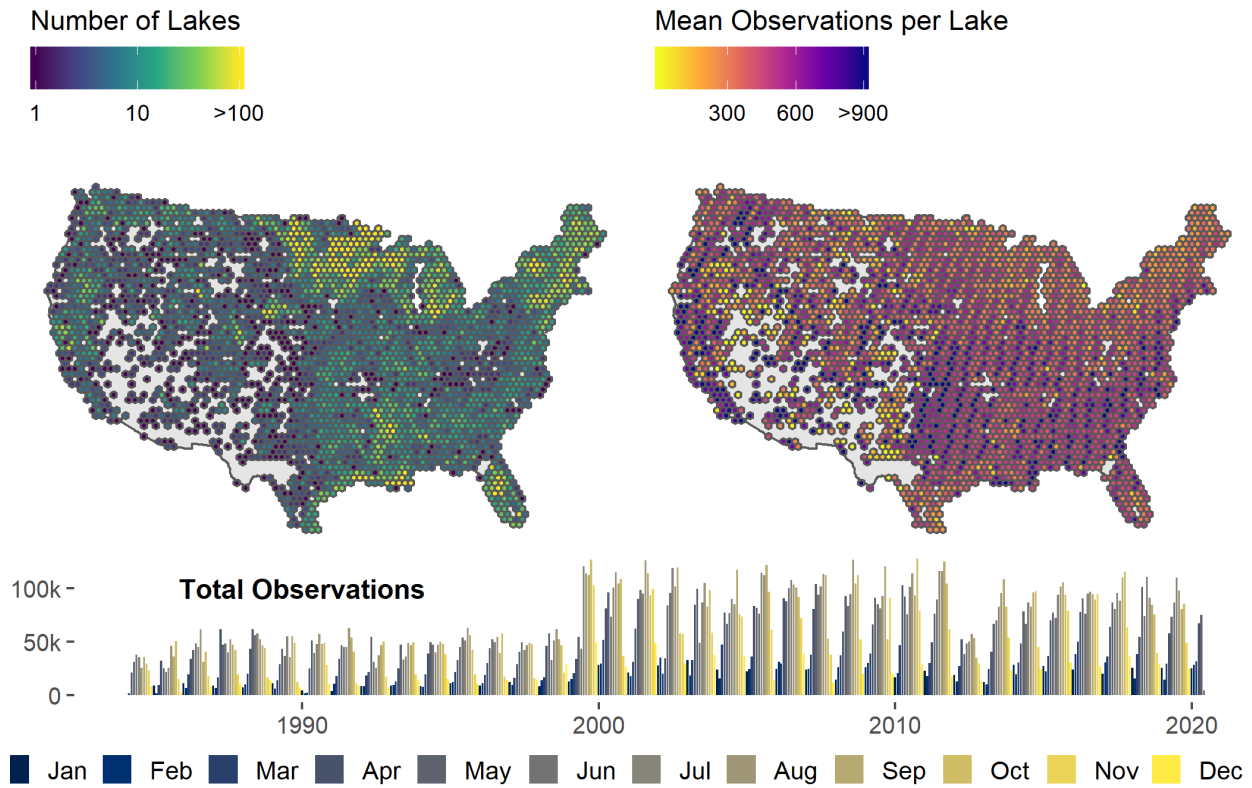
Figure 2. Temporal and spatial distributions of satellite observations contained within the LimnoSat-US database.

3.1 Classes of lake color phenology.

Our final clustering partitions resulted in one of three membership classes for each lake/period that was not *a priori* classified as aseasonal (Figure 3). We describe these groups as Spring Greening, Summer Greening, or Bimodal. High mean Jaccard Similarity Indices across bootstrap sampling iterations (0.77, 0.80, 0.94 respectively) show these clusters are relatively universal, and that regardless of the initial sample, the same lakes are consistently clustered together. Within these clusters, we refer to red-shifted portions of the time series (increasing values) as greening or green-shifted and blue shifted portions of the time series (decreasing values) as blueing or blue-shifted. We highlight this terminology because even though red is the end-member of the upper wavelengths, the vast majority of the colors do not extend beyond the green portion of the spectrum. Descriptions of the summary attributes for each cluster are as follows:

1) Spring Greening (n = 55,378, 35.4%): Lake color is green-shifted in May/June and gradually moves towards the blue end of the spectrum throughout the summer and fall months. Median dominant wavelengths for these phenologies are significantly bluer (p < 0.0001) than those in the Summer Greening, Bimodal, or Aseasonal clusters (median λ_d = 513). They have the highest average coefficient of variation within each individual time series (p < 0.0001), with an average range of 37 nm for a given lake/period compared to 34 nm, 33 nm, and 12 nm for Summer Greening, Bimodal, and Aseasonal clusters, respectively. The distribution of colors within the

304   cluster is concentrated around a mode 498 nm and skewed towards the greener portion of the
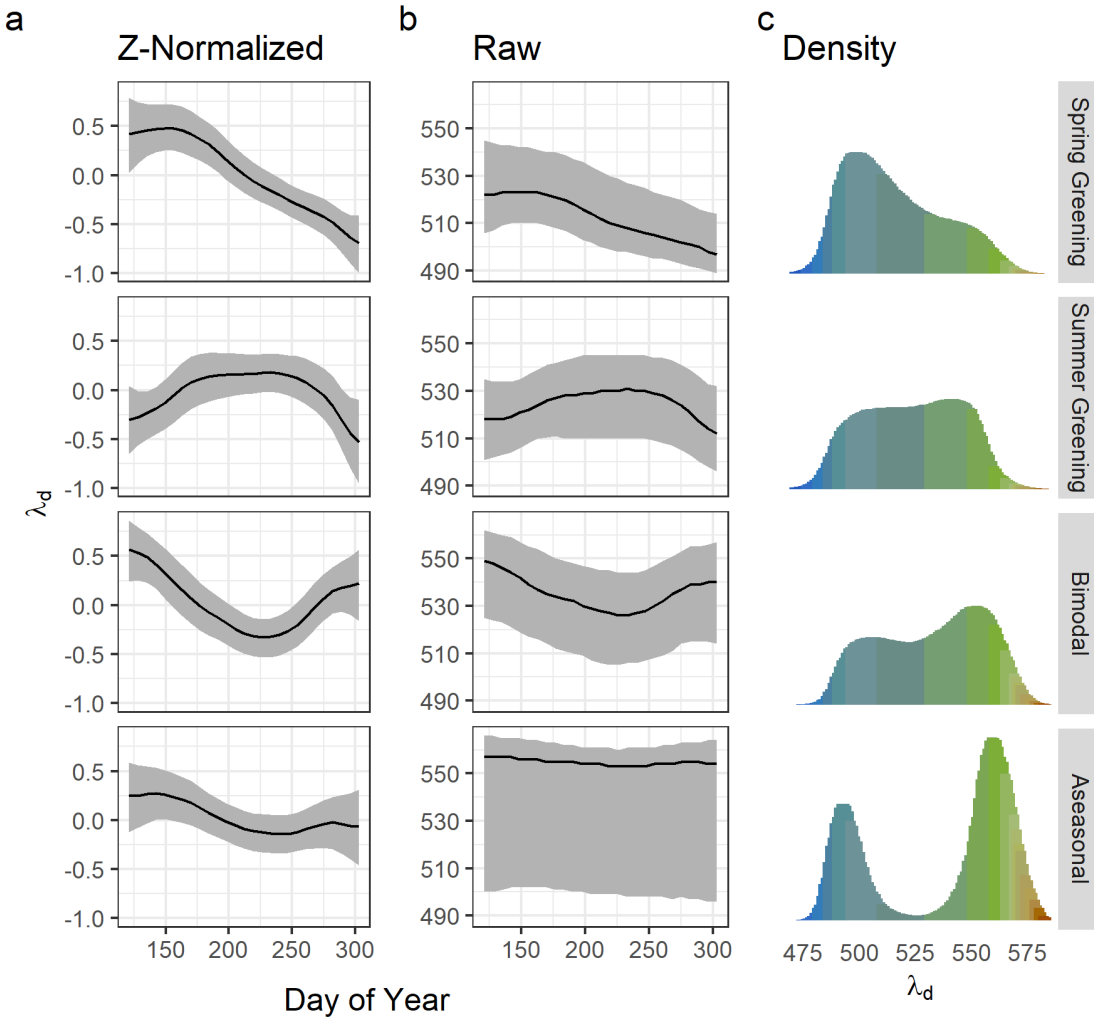spectrum.

306

Figure 3. Results of cluster analysis for over 26,000 lakes and 156,000 seasonal time series.
308   Black lines represent medians with grey ribbons representing the 1st-3rd quartile of each cluster.
Clusters are shown both in their (a) z-normalized form used in the cluster analysis and (b) their
310   raw dominant wavelength form. Distributions of color observations in each cluster are displayed
using their associated Forel-Ule Index color. Note that the range of wavelengths associated with
312   each Forel-Ule Index value varies.

314   2) Summer greening (n = 24,580, 15.7%): Lake color is characterized by gradual greening from
May-August after which time it drops towards the blue end of the color spectrum. The
316   distribution of colors shows a mode of 542 nm and a median of 524 nm with a blue-skewed
distribution. On average, each individual time series within this class shows significantly less
318   variation than Spring Greening lakes/periods (p < 0.0001) but no significant difference from
Bimodal lakes/periods.

320 3) Bimodal (n = 29,685, 19.0%): Lake color is most green-shifted in May/June and again in September/October, with a somewhat blue-shifted phase in the intervening months. Phenologies
322 within this cluster are significantly more green-shifted (p < 0.0001) than lakes within either the Spring or Summer Greening clusters and show less variation (p < 0.0001) than those in the
324 Spring Greening clusters. The distribution of colors is concentrated around 553 nm with a much less pronounced peak at 507 nm.

326 4) Aseasonal (n = 46,759, 29.9%): The overall color distribution of this cluster is distinctly bimodal, with a primary mode at 559 nm and a secondary mode at 492 nm. This bimodal
328 distribution, combined with the small variance in any given lake/period in the cluster, suggests it contains predominantly blue and predominantly green time series with very few observations in
330 the intermediate green/blue space common within the three other clusters. The cluster also contains both the most green-shifted and most blue-shifted time series included within the
332 analyses. Because of the crisp partition contained within the cluster and the ecological significance of blue versus green aseasonal time series, we further partition this cluster into
334 Aseasonal (Blue) (n = 15,934) and Aseasonal (Green) (n = 30,825) lakes for the remainder of the analysis. Time series with a median dominant wavelength less than or greater than the anti-mode
336 of the distribution (525 nm) are considered Aseasonal (Blue) and Aseasonal (Green) respectively.

338   3.3 Lake stability over time

 Aseasonal Green lakes showed the most stability over time, with an average of 73% +/- 6%
340 (mean +/- standard deviation) of lakes remaining within the cluster between consecutive time periods. Aseasonal (Blue) and Spring Greening clusters showed similar retention rates of 57%
342 +/- 17% and 57% +/- 9% respectively, while Bimodal and Summer Greening showed similar retention rates of 46% +/- 8% and 45% +/- 7%. However, of these, only the differences between
344 Aseasonal (Green) and Bimodal/Summer Greening clusters were statistically significant at a 95% confidence interval. For Spring Greening, Aseasonal (Green), and Aseasonal (Blue)
346 distributions, the number of lakes retained between each period was significantly higher than the number of lakes that transitioned to a different cluster (p = 0.047, p = 0.007, and p = 0.0001
348 respectively). Summer Greening and Bimodal clusters showed no significant difference between the proportion of lakes retained and lakes that transitioned to other clusters, indicating less
350 stability than the other three classes. However, these transitions showed distinct patterns, with lakes transitioning more commonly between similar clusters. As an example, on average 27% of
352 Summer Greening lakes transitioned to Spring Greening lakes between periods, but only 4% of Summer Greening lakes transitioned to Aseasonal (Green) (Figure 4). Similarly, less than 0.2%
354 of lakes in Aseasonal (Green) and Aseasonal (Blue) transitioned between the two clusters in any two consecutive periods indicating that state shifts between dominantly blue lakes and
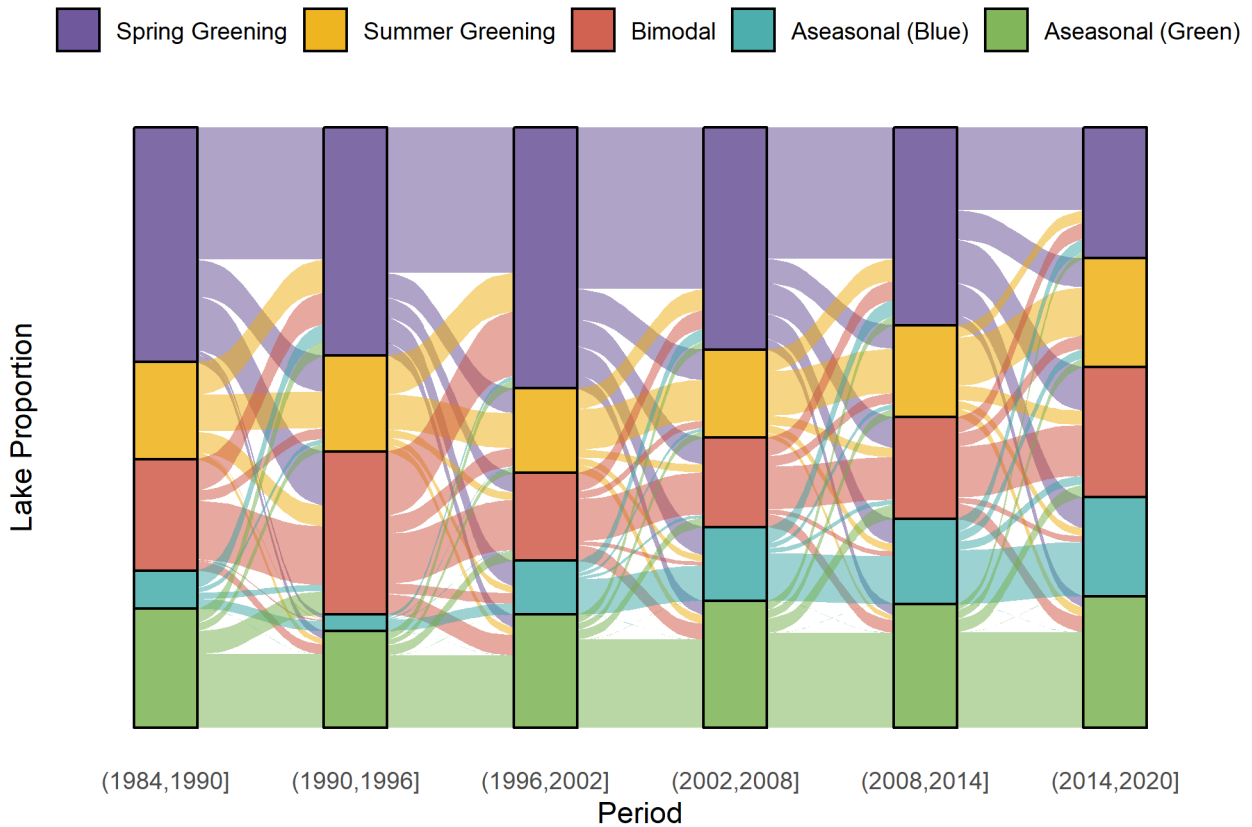356 dominantly green lakes are very uncommon.

358

360

Figure 4. Sankey diagram showing the distribution of lake phenology transitions between periods. Each ribbon is proportional to the number of lakes that moved from one cluster class to another.

Lake stability, or the number of times a lake moved from one class to another (ranging from 0 transitions to 5), showed that lakes with three transitions were most common (n = 6,458) and lakes with five transitions least common (n = 1254) (Figure S5). We also calculated the number of unique clusters a lake occupied throughout its transitions. For instance, a lake could change states between all five periods, giving it a stability score of five, but only be changing between two of the potential five clusters, giving it two unique states. Of the 26,067 lakes, 4,339 (16.6%) remained within the same cluster through all periods while only 21 (< 0.1%) occupied all five clusters at some point. For those lakes in between, lakes occupying two distinct states (n = 11,091; 42.5%) were most common followed by three states (n = 8,942; 34.3%) and four states (n = 1,674; 6.5%) respectively. Linear regressions between lake and landscape level metrics with overall lake stability showed significant relationships (p <0.01) with 5 out of 26 possible metrics (Table S1), although some of these metrics have significant cross-correlation (Figure S6).

4 Discussion

4.1 - Lake seasonal phenology types

380   Existing paradigms regarding the seasonality of lake color are generally derived from individual lakes with rich sampling histories of water quality observations; however these long-term field

382   records are rare and limited to a small subsample of lakes (Stanley et al., 2019). While these data-rich study lakes are essential for understanding fine-scale ecosystem processes, they lack

384   the spatial coverage to generalize across entire landscapes (Collins et al., 2019; Soranno et al., 2014). Within our clustering analysis, we found that lake color phenology can largely be

386   categorized as Aseasonal, Spring Greening, Summer Greening, or Bimodal. These phenologies show distinct regional patterns and spatial auto-correlation, with the probability of two lakes

388   being in the same cluster showing a significant relationship to the distance between those two lakes ($p < 0.0001$) up to a distance of ~1,500 km (Figure 5b).

390   Each cluster has a unique distribution of dominant wavelengths (Figure 3), which suggests that the timing of seasonal variation in color is connected with lake biogeochemistry. This conclusion

392   is supported by long-standing models of freshwater phytoplankton succession (Sommer et al., 1986) and observations of annual cycles of chlorophyll-a, a proxy for phytoplankton biomass

394   (Winder & Cloern, 2010). Oligotrophic temperate lakes often show the archetypal pattern of a spring phytoplankton bloom followed by low summer concentrations. This was the dominant

396   phenology in our observations (35.4%), which is in-line with a study of 125 aquatic systems that found that nearly half of the sites displayed a dominant 12-month cycle with one phytoplankton

398   peak per year (Winder & Cloern, 2010). As nutrient availability increases, eutrophic lakes tend to experience discrete phytoplankton blooms in the spring and late-summer/fall (Marshall &

400   Peters, 1989). This pattern is captured in our Bimodal cluster, where the raw dominant wavelength values are significantly greener than those in any other cluster except for Aseasonal

402   (Green). The summer-greening cluster captures eutrophic to hyper-eutrophic lakes featuring prolonged summer blooms with highly variable summer algal concentrations (Carpenter et al.,

404   2020; Huisman et al., 2018). The characterization of Bimodal and Summer Greening lakes/periods as eutrophic is further supported by the low levels of variation we observe in

406   dominant wavelengths when compared to Spring Greening lakes/periods. Dominant wavelength saturates with high amounts of suspended matter, chl-a, and/or CDOM (Bukata et al., 1997),

408   meaning that highly productive, algae-filled lakes with significant amounts of these constituents would show low variation as dominant wavelength saturates. It is also possible that lakes in

410   these categories are dystrophic CDOM-dominated lakes, as they include some of the most red-shifted (brown) waterbodies within the study.
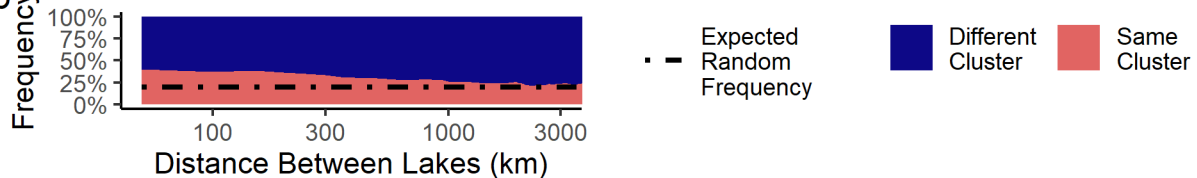
a
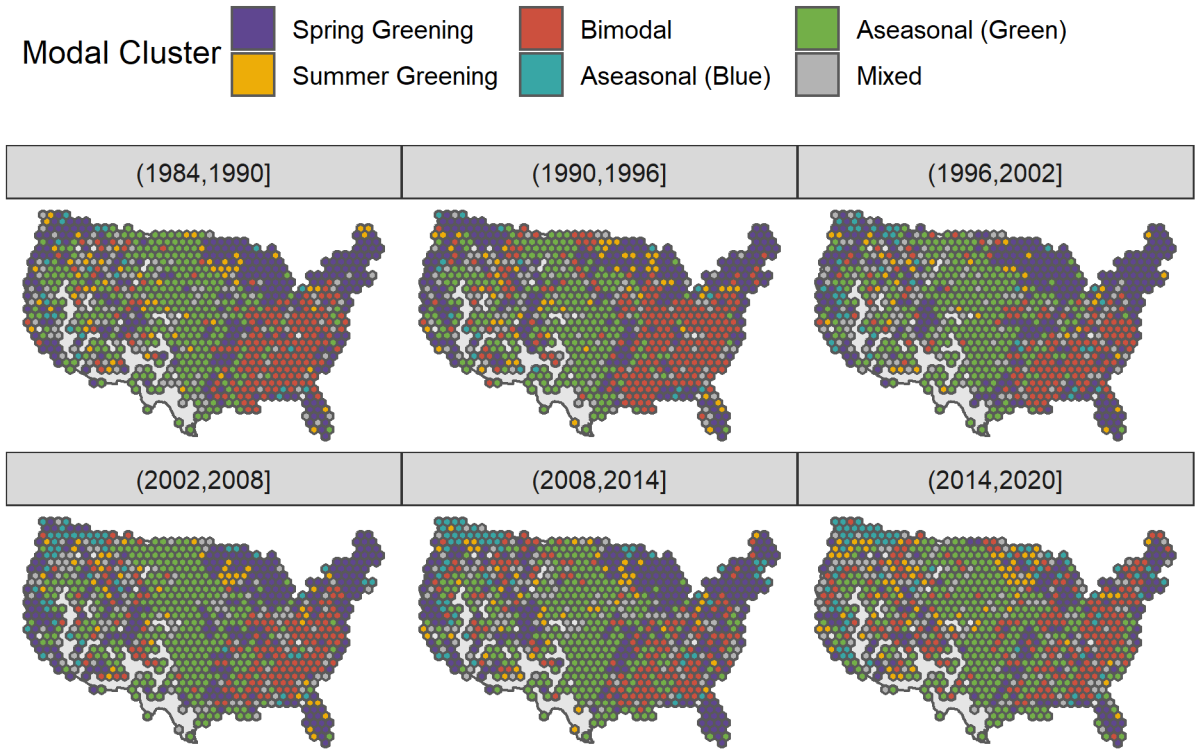
Figure 5. a) The modal cluster within each 100 km x 100 km grid across time periods. Mixed grids are those where there is no dominant cluster (i.e. two or more clusters are equally prevalent). b) The frequency of same cluster pairs to different cluster pairs using each lake's modal cluster. The frequency distributions were calculated within 50 km windows for a random sample of 30% of the study lakes. The dotted line represents the expected frequency if the distribution was random without any spatial autocorrelation.

The proportion of lakes that fall within different clusters does not show an overall trend over time; however, since the 1996-2002 period, the number of lakes classified as either Bimodal or Aseasonal (Blue) have increased while the number classified as Spring Greening have been decreasing (Figures 4, 5). Much of the increase in Aseasonal (Blue) lakes is concentrated in the

424 Pacific Northwest and occurred prior to 2008, whereas the decrease in Spring Greening Lakes has predominantly occurred in higher-latitude lakes that may be more sensitive to changes in

426 snowmelt and ice cover regimes which control nutrient and sediment fluxes that influence lake productivity (Gerten & Adrian, 2002; Sharma et al., 2019). Patterns in the Aseasonal (Green)

428 cluster show much less variation both spatially and temporally, being largely concentrated in the agriculturally dominated central and northern plains and showing no distinct temporal pattern in

430 quantity. While the increase in Aseasonal (Blue) lakes is potentially indicative of reduced sediment and nutrient inputs in certain parts of the country, the increase in Bimodal lakes, when

432 taken with its close match to eutrophic phytoplankton succession patterns, indicates increases in lake productivity across portions of the U.S. since the mid 1990s. This pattern supports recent

434 research showing a transition from bluer lakes to murky chlorophyll-a and CDOM-dominated lakes throughout the US between 2007 and 2012 (Leech et al., 2018). However, dominant

436 wavelength, and optical water color more generally, is controlled by a variety of optically active water color constituents in addition to phytoplankton (Gholizadeh et al., 2016; Mobley, 1994),

438 and partitioning these optical components is beyond the scope of this analysis. The result does, however, merit further research using a database like LimnoSat-US to examine country wide

440 trends in lake chlorophyll-a content.

4.3 - Factors influencing lake stability over time

442 Lake stability, or the number of times a lake moved between clusters during the study period, showed significant relationships with multiple lake and landscape level metrics from

444 HydroLAKES and the GLCP database (Figure 6, Table S1). These relationships can generally be categorized as either hydrological properties or landscape properties. Important hydrological

446 properties related to stability include lake size and discharge (both positively correlated with stability). This result supports existing research suggesting that larger water bodies are less

448 reactive to perturbations than smaller, shallower lakes that can fluctuate among multiple productivity regimes (Scheffer & van Nes, 2007). We also find that hydrologically dynamic

450 lakes are consistently less stable, with lakes showing large interannual variations in seasonal surface extent exhibiting less stability. It is likely that these hydrologically dynamic lakes are

452 more sensitive to seasonal variations in runoff and resuspension of lakebed sediments leading to large interannual variations in nutrient and sediment load.

454 The landscape level metrics that showed the strongest relationship with lake stability were catchment population and elevation ($p < 0.01$) followed by mean temperature and mean monthly

456 precipitation ($p < 0.05$). Similarly, for the subset of these variables where we had observations at annual timescales, we found that high coefficients of variation between years (interannual

458 variation) of these metrics showed strong linear relationships to stability. The impact of these landscape-level metrics on stability supports work showing that lakes integrate surrounding

460 climatic and land cover changes (Rose et al., 2017). These results are of particular interest for relatively pristine high-elevation lakes that will be disproportionately impacted by changing

462 precipitation and temperature regimes through climate change (Oleksy, Baron, et al., 2020; Oleksy, Beck, et al., 2020). Finally, we found that lakes in catchments with higher populations

464 were generally more stable; however, lakes in catchments with high variation in population (likely increasing urban areas) showed less stability. Overall, our examination of landscape level

466 metrics shows that the stability of a lake often follows the stability of its environment, with lakes subject to interannual variations in climate or anthropogenic stressors generally showing less
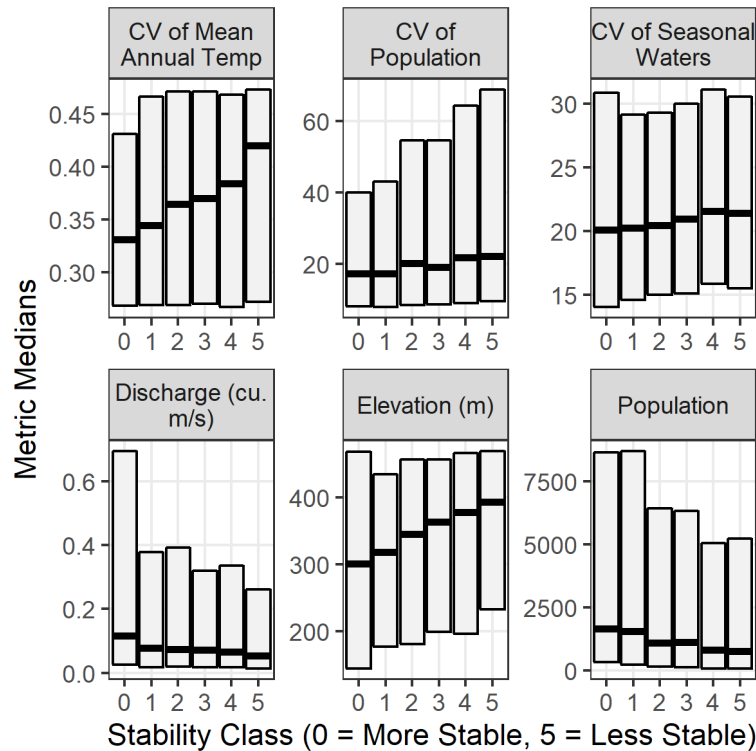
468 stability in their overall seasonal phenology.

Figure 6. Lake and landscape level metrics that showed the most significant relationships with stability, or the number of times a given lake moved from one cluster to another between periods ($p < 0.01$ with the exception of discharge, $p = 0.019$). Center bars represent median values while boxes span the 1st-3rd quartiles.

5. Conclusion

Remote sensing has the capability to substantially increase our understanding of macroscale aquatic ecosystem processes. Here, we contribute to a growing body of inland water remote sensing resources with LimnoSat-US, which contains >22,000,000 remotely sensed lake observations. Prior to this study, large-scale analyses of lake phenologies were limited to dozens to hundreds of waterbodies (Ho et al., 2019; Marshall & Peters, 1989; Winder & Cloern, 2010). Here, we were able to analyze U.S. summer lake color phenology across more than 26,000 lakes over 36 years, showing both temporal and spatial patterns and trends, as well as linking phenology to lake and landscape-level metrics. Better understanding the full distribution of lake phenology will allow for more accurate scaling of global nutrient and carbon cycling. While the analysis presented here relies simply on lake color, combining LimnoSat-US with databases such as AquaSat (Ross et al., 2019), RiverSR (Gardner et al., 2020), and LIMNADES (Spyrakos et al., 2020), will allow for more explicit modelling and analysis of specific water quality components, allowing researchers to partition the patterns observed here into optically active water quality components including chlorophyll-a, suspended sediments, and CDOM.

490   **Acknowledgments**

References

Allen, G. H., Yang, X., Gardner, J., Holliman, J., David, C. H., & Ross, M. (2020). Timing of Landsat overpasses effectively captures flow conditions of large rivers. *Remote Sensing*, *12*(9), 1510. https://doi.org/10.3390/rs12091510

Arbelaitz, O., Gurrutxaga, I., Muguerza, J., Pérez, J. M., & Perona, I. (2013). An extensive comparative study of cluster validity indices. *Pattern Recognition*, *46*(1), 243–256. https://doi.org/10.1016/j.patcog.2012.07.021

Barysheva, L. (1987). On the issue of intercorrespondence of color scales used in limnology. *Remote Monitoring of Large Lakes*, 60–65.

Binding, C. E., Jerome, J. H., Bukata, R. P., & Booty, W. G. (2007). Trends in water clarity of the lower Great Lakes from remotely sensed aquatic color. *Journal of Great Lakes Research*, *33*(4), 828–841. https://doi.org/10.3394/0380-1330(2007)33[828:TIWCOT]2.0.CO;2

Brunner, M. I., Melsen, L. A., Newman, A. J., Wood, A. W., & Clark, M. P. (2020). Future streamflow regime changes in the United States: assessment using functional classification. *Hydrology and Earth System Sciences*, *24*(8), 3951–3966. https://doi.org/10.5194/hess-24-3951-2020

Bukata, R. P., Jerome, J. H., Kondratyev, K. Ya., Pozdnyakov, D. V., & Kotykhov, A. A. (1997). Modelling the radiometric color of inland waters: Implications to a) remote sensing and b) limnological color scales. *Journal of Great Lakes Research*, *23*(3), 254–269. https://doi.org/10.1016/S0380-1330(97)70910-9

Byrnes, D. K., Meter, K. J. V., & Basu, N. B. (2020). Long-term shifts in U.S. nitrogen sources and sinks revealed by the new TREND-Nitrogen data set (1930–2017). *Global Biogeochemical Cycles*, *34*(9), e2020GB006626. https://doi.org/10.1029/2020GB006626

Cao, Z., Ma, R., Duan, H., Pahlevan, N., Melack, J., Shen, M., & Xue, K. (2020). A machine learning approach to estimate chlorophyll-a from Landsat-8 measurements in inland lakes. *Remote Sensing of Environment*, *248*, 111974. https://doi.org/10.1016/j.rse.2020.111974

Carpenter, S. R., Arani, B. M. S., Hanson, P. C., Scheffer, M., Stanley, E. H., & Nes, E. V. (2020). Stochastic dynamics of Cyanobacteria in long-term high-frequency observations of a eutrophic lake. *Limnology and Oceanography Letters*, *5*(5), 331–336. https://doi.org/10.1002/lol2.10152

Collins, S. M., Yuan, S., Tan, P. N., Oliver, S. K., Lapierre, J. F., Cheruvelil, K. S., et al. (2019). Winter precipitation and summer temperature predict lake water quality at macroscales. *Water Resources Research*, *55*(4), 2708–2721. https://doi.org/10.1029/2018WR023088

Davies, D. L., & Bouldin, D. W. (1979). A cluster separation measure. *IEEE Transactions on Pattern Analysis and Machine Intelligence*, *PAMI-1*(2), 224–227. https://doi.org/10.1109/TPAMI.1979.4766909

Dekker, A. G., & Peters, S. W. M. (1993). The use of the thematic mapper for the analysis of eutrophic lakes: A case study in the Netherlands. *International Journal of Remote Sensing*, *14*(5), 799–821. https://doi.org/10.1080/01431169308904379

Dekker, A. G., Vos, R. J., & Peters, S. W. M. (2001). Comparison of remote sensing data, model results and in situ data for total suspended matter (TSM) in the southern Frisian lakes. *Science of the Total Environment*, *268*(1–3), 197–214. https://doi.org/10.1016/S0048-9697(00)00679-3

546 Dethier, E. N., Renshaw, C. E., & Magilligan, F. J. (2020). Toward improved accuracy of remote sensing approaches for quantifying suspended sediment: Implications for suspended-sediment monitoring. *Journal of Geophysical Research: Earth Surface*, *125*(7),
548 e2019JF005033. https://doi.org/10.1029/2019JF005033

Dunn, O. J. (1961). Multiple comparisons among means. *Journal of the American Statistical*
550 *Association*, *56*(293), 52–64. https://doi.org/10.2307/2282330

Dwyer, J. L., Roy, D. P., Sauer, B., Jenkerson, C. B., Zhang, H. K., & Lymburner, L. (2018).
552 Analysis ready data: Enabling analysis of the landsat archive. *Remote Sensing*, *10*(9), 1–19. https://doi.org/10.3390/rs10091363

554 Gardner, J., Yang, X., Topp, S., Ross, M., & Pavelsky, T. (2020). River Surface Reflectance (riverSR) Database [Data set]. Zenodo. https://doi.org/10.5281/zenodo.3838387

556 Gerten, D., & Adrian, R. (2002). Effects of climate warming, North Atlantic Oscillation, and El Niño-Southern Oscillation on thermal conditions and plankton dynamics in Northern
558 Hemispheric lakes. *The Scientific World JOURNAL*, *2*, 586–606. https://doi.org/10.1100/tsw.2002.141

560 Gholizadeh, M., Melesse, A., & Reddi, L. (2016). A comprehensive review on water quality parameters estimation using remote sensing techniques. *Sensors*, *16*(8), 1298.
562 https://doi.org/10.3390/s16081298

Giardino, C., Kõks, K.-L., Bolpagni, R., Luciani, G., Candiani, G., Lehmann, M. K., et al.
564 (2019). The color of water from space: A case study for Italian lakes from Sentinel-2. *Geospatial Analyses of Earth Observation (EO) Data*.
566 https://doi.org/10.5772/intechopen.86596

Gorelick, N., Hancher, M., Dixon, M., Ilyushchenko, S., Thau, D., & Moore, R. (2017). Google
568 Earth Engine: Planetary-scale geospatial analysis for everyone. *Remote Sensing of Environment*. https://doi.org/10.1016/j.rse.2017.06.031

570 Griffin, C. G., McClelland, J. W., Frey, K. E., Fiske, G., & Holmes, R. M. (2018). Quantifying CDOM and DOC in major Arctic rivers during ice-free conditions using Landsat TM and
572 ETM+ data. *Remote Sensing of Environment*, *209*, 395–409. https://doi.org/10.1016/j.rse.2018.02.060

574 Heathcote, A. J., & Downing, J. A. (2012). Impacts of eutrophication on carbon burial in freshwater lakes in an intensively agricultural landscape. *Ecosystems*, *15*(1), 60–70.
576 https://doi.org/10.1007/s10021-011-9488-9

Ho, J. C., Michalak, A. M., & Pahlevan, N. (2019). Widespread global increase in intense lake
578 phytoplankton blooms since the 1980s. *Nature*, *574*(7780), 667–670. https://doi.org/10.1038/s41586-019-1648-7

580 Hollander, M., & Wolfe, D. A. (1973). In *Nonparametric Statistical Methods, 3rd Edition* (pp. 115–120). New York: John Wiley & Sons. Retrieved from https://www.wiley.com/en-
582 us/Nonparametric+Statistical+Methods%2C+3rd+Edition-p-9780470387375

Huisman, J., Codd, G. A., Paerl, H. W., Ibelings, B. W., Verspagen, J. M. H., & Visser, P. M.
584 (2018). Cyanobacterial blooms. *Nature Reviews Microbiology*, *16*(8), 471–483. https://doi.org/10.1038/s41579-018-0040-1

586 Jain, A. K., & Moreau, J. V. (1987). Bootstrap technique in cluster analysis. *Pattern Recognition*, *20*(5), 547–568. https://doi.org/10.1016/0031-3203(87)90081-1

588 Jones, J. W. (2015). Efficient wetland surface water detection and monitoring via Landsat: Comparison with in situ data from the Everglades Depth Estimation Network. *Remote*
590 *Sensing*, *7*(9), 12503–12538. https://doi.org/10.3390/rs70912503

Jones, J. W. (2019). Improved automated detection of subpixel-scale inundation—revised dynamic surface water extent (DSWE) partial surface water tests. *Remote Sensing*, *11*(4), 374. https://doi.org/10.3390/rs11040374

Keogh, E., & Kasetty, S. (2003). On the need for time series data mining benchmarks: a survey and empirical demonstration. *Data Mining and Knowledge Discovery*, *7*(4), 349–371.

Kim, M., & Ramakrishna, R. S. (2005). New indices for cluster validity assessment. *Pattern Recognition Letters*, *26*(15), 2353–2363. https://doi.org/10.1016/j.patrec.2005.04.007

Knoll, L. B., Williamson, C. E., Pilla, R. M., Leach, T. H., Brentrup, J. A., & Fisher, T. J. (2018). Browning-related oxygen depletion in an oligotrophic lake. *Inland Waters*, *8*(3), 255–263. https://doi.org/10.1080/20442041.2018.1452355

Kuhn, C., de Matos Valerio, A., Ward, N., Loken, L., Sawakuchi, H. O., Kampel, M., et al. (2019). Performance of Landsat-8 and Sentinel-2 surface reflectance products for river remote sensing retrievals of chlorophyll-a and turbidity. *Remote Sensing of Environment*, *224*, 104–118. https://doi.org/10.1016/j.rse.2019.01.023

Kuhn, C. D., Bogard, M., Johnston, S. E., John, A., Vermote, E. F., Spencer, R., et al. (2020). Satellite and airborne remote sensing of gross primary productivity in boreal Alaskan lakes. *Environmental Research Letters*. https://doi.org/10.1088/1748-9326/aba46f

Leech, D. M., Pollard, A. I., Labou, S. G., & Hampton, S. E. (2018). Fewer blue lakes and more murky lakes across the continental U.S.: Implications for planktonic food webs. *Limnology and Oceanography*, 1–20. https://doi.org/10.1002/LNO.10967

Maberly, S. C., O'Donnell, R. A., Woolway, R. I., Cutler, M. E. J., Gong, M., Jones, I. D., et al. (2020). Global lake thermal regions shift under climate change. *Nature Communications*, *11*(1), 1232. https://doi.org/10.1038/s41467-020-15108-z

Marshall, C. T., & Peters, R. H. (1989). General patterns in the seasonal development of chlorophyll a for temperate lakes. *Limnology and Oceanography*, *34*(5), 856–867. https://doi.org/10.4319/lo.1989.34.5.0856

Martinuzzi, S., Januchowski-Hartley, S. R., Pracheil, B. M., McIntyre, P. B., Plantinga, A. J., Lewis, D. J., & Radeloff, V. C. (2014). Threats and opportunities for freshwater conservation under future land use change scenarios in the United States. *Global Change Biology*, *20*(1), 113–124. https://doi.org/10.1111/gcb.12383

Masek, J. G., Vermote, E. F., Saleous, N. E., Wolfe, R., Hall, F. G., Huemmrich, K. F., et al. (2006). A Landsat surface reflectance dataset for North America, 1990-2000. *IEEE Geoscience and Remote Sensing Letters*, *3*(1), 68–72. https://doi.org/10.1109/LGRS.2005.857030

Matsuzaki, S.-I. S., Lathrop, R. C., Carpenter, S. R., Walsh, J. R., Zanden, M. J. V., Gahler, M. R., & Stanley, E. H. (2020). Climate and food web effects on the spring clear-water phase in two north-temperate eutrophic lakes. *Limnology and Oceanography*, *n/a*(n/a). https://doi.org/10.1002/lno.11584

McCullough, I. M., Loftin, C. S., & Sader, S. A. (2013). Landsat imagery reveals declining clarity of Maine's lakes during 1995–2010. *Freshwater Science*, *32*(3), 741–752. https://doi.org/10.1899/12-070.1

Messager, M. L., Lehner, B., Grill, G., Nedeva, I., & Schmitt, O. (2016). Estimating the volume and age of water stored in global lakes using a geo-statistical approach. *Nature Communications*, *7*, 1–11. https://doi.org/10.1038/ncomms13603

Meyer, M. F., Labou, S. G., Cramer, A. N., Brousil, M. R., & Luff, B. T. (2020). The global lake area, climate, and population dataset. *Scientific Data*, *7*(1), 174. https://doi.org/10.1038/s41597-020-0517-4

Mobley, C. (1994). Chapter 3: Optical Properties of Water. In *Light and Water: Radiative Transfer in Natural Waters* (pp. 60–144). Academic Press.

Monteith, D. T., Stoddard, J. L., Evans, C. D., de Wit, H. A., Forsius, M., Høgåsen, T., et al. (2007). Dissolved organic carbon trends resulting from changes in atmospheric deposition chemistry. *Nature*, *450*(7169), 537–540. https://doi.org/10.1038/nature06316

Mueen, A., & Keogh, E. (2016). Extracting optimal performance from dynamic time warping. In *Proceedings of the 22nd ACM SIGKDD International Conference on Knowledge Discovery and Data Mining* (pp. 2129–2130).

Müller, B., Bryant, L. D., Matzinger, A., & Wüest, A. (2012). Hypolimnetic oxygen depletion in eutrophic lakes. *Environmental Science & Technology*, *46*(18), 9964–9971. https://doi.org/10.1021/es301422r

Nadaraya, E. A. (1964). On estimating regression. *Theory of Probability & Its Applications*, *9*(1), 141–142. https://doi.org/10.1137/1109020

Oleksy, I. A., Baron, J. S., Leavitt, P. R., & Spaulding, S. A. (2020). Nutrients and warming interact to force mountain lakes into unprecedented ecological states. *Proceedings of the Royal Society B: Biological Sciences*, *287*(1930), 20200304. https://doi.org/10.1098/rspb.2020.0304

Oleksy, I. A., Beck, W. S., Lammers, R. W., Steger, C. E., Wilson, C., Christianson, K., et al. (2020). The role of warm, dry summers and variation in snowpack on phytoplankton dynamics in mountain lakes. *Ecology*. https://doi.org/10.1002/ecy.3132

Olmanson, L. G., Bauer, M. E., & Brezonik, P. L. (2008). A 20-year Landsat water clarity census of Minnesota's 10,000 lakes. *Remote Sensing of Environment*, *112*(11), 4086–4097. https://doi.org/10.1016/j.rse.2007.12.013

Olmanson, L. G., Page, B. P., Finlay, J. C., Brezonik, P. L., Bauer, M. E., Griffin, C. G., & Hozalski, R. M. (2020). Regional measurements and spatial/temporal analysis of CDOM in 10,000+ optically variable Minnesota lakes using Landsat 8 imagery. *Science of The Total Environment*, *724*, 138141. https://doi.org/10.1016/j.scitotenv.2020.138141

O'Reilly, C. M., Sharma, S., Gray, D. K., Hampton, S. E., Read, J. S., Rowley, R. J., et al. (2015). Rapid and highly variable warming of lake surface waters around the globe. *Geophysical Research Letters*, *42*(24), 10,773-10,781. https://doi.org/10.1002/2015GL066235

Ritchie, J. C., & Cooper, C. M. (1988). Comparison of measured suspended sediment concentrations with suspended sediment concentrations estimated from Landsat MSS data. *International Journal of Remote Sensing*, *9*(3), 379–387. https://doi.org/10.1080/01431168808954861

Rose, K. C., Greb, S. R., Diebel, M., & Turner, M. G. (2017). Annual precipitation regulates spatial and temporal drivers of lake water clarity: *Ecological Applications*, *27*(2), 632–643. https://doi.org/10.1002/eap.1471

Ross, M. R. V., Topp, S. N., Appling, A. P., Yang, X., Kuhn, C., Butman, D., et al. (2019). AquaSat: A data set to enable remote sensing of water quality for inland waters. *Water Resources Research*, *55*(11), 10012–10025. https://doi.org/10.1029/2019WR024883

Roulet, N., & Moore, T. R. (2006). Browning the waters. *Nature*, *444*(7117), 283–284. https://doi.org/10.1038/444283a

Roy, D. P., Kovalskyy, V., Zhang, H. K., Vermote, E. F., Yan, L., Kumar, S. S., & Egorov, A. (2016). Characterization of Landsat-7 to Landsat-8 reflective wavelength and normalized difference vegetation index continuity. *Remote Sensing of Environment*, *185*, 57–70. https://doi.org/10.1016/j.rse.2015.12.024

Savoy, P., Appling, A. P., Heffernan, J. B., Stets, E. G., Read, J. S., Harvey, J. W., & Bernhardt, E. S. (2019). Metabolic rhythms in flowing waters: An approach for classifying river productivity regimes. *Limnology and Oceanography*, *64*(5), 1835–1851. https://doi.org/10.1002/lno.11154

Scheffer, M., & van Nes, E. H. (2007). Shallow lakes theory revisited: various alternative regimes driven by climate, nutrients, depth and lake size. *Hydrobiologia*, *584*(1), 455–466. https://doi.org/10.1007/s10750-007-0616-7

Sharma, S., Blagrave, K., Magnuson, J. J., O'Reilly, C. M., Oliver, S., Batt, R. D., et al. (2019). Widespread loss of lake ice around the Northern Hemisphere in a warming world. *Nature Climate Change*, *9*(3), 227–231. https://doi.org/10.1038/s41558-018-0393-5

Shen, Z., Yu, X., Sheng, Y., Li, J., & Luo, J. (2015). A fast algorithm to estimate the deepest points of lakes for regional lake registration. *PLOS ONE*, *10*(12), e0144700. https://doi.org/10.1371/journal.pone.0144700

Sommer, U., Gliwicz, Z. M., Lampert, W., & Duncan, A. (1986). The PEG-model of seasonal succession of planktonic events in fresh waters. *Arch. Hydrobiol*, *106*(4), 433–471.

Sommer, U., Adrian, R., De Senerpont Domis, L., Elser, J. J., Gaedke, U., Ibelings, B., et al. (2012). Beyond the Plankton Ecology Group (PEG) Model: Mechanisms Driving Plankton Succession. *Annual Review of Ecology, Evolution, and Systematics*, *43*, 429–448.

Soranno, P. A., Cheruvelil, K. S., Bissell, E. G., Bremigan, M. T., Downing, J. A., Fergus, C. E., et al. (2014). Cross-scale interactions: Quantifying multi-scaled cause-effect relationships in macrosystems. *Frontiers in Ecology and the Environment*, *12*(1), 65–73. https://doi.org/10.1890/120366

Soranno, P. A., Bacon, L. C., Beauchene, M., Bednar, K. E., Bissell, E. G., Boudreau, C. K., et al. (2017). LAGOS-NE: A multi-scaled geospatial and temporal database of lake ecological context and water quality for thousands of U.S. lakes. *GigaScience*, (October 2017), 1–22. https://doi.org/10.1093/gigascience/gix101

Spyrakos, E., Hunter, P., Simis, S., Neil, C., Riddick, C., Wang, S., et al. (2020). Moving towards global satellite based products for monitoring of inland and coastal waters. Regional examples from Europe and South America. In *2020 IEEE Latin American GRSS ISPRS Remote Sensing Conference (LAGIRS)* (pp. 363–368). https://doi.org/10.1109/LAGIRS48042.2020.9165653

Stanley, E. H., Collins, S. M., Lottig, N. R., Oliver, S. K., Webster, K. E., Cheruvelil, K. S., & Soranno, P. A. (2019). Biases in lake water quality sampling and implications for macroscale research. *Limnology and Oceanography*, *64*(4), 1572–1585. https://doi.org/10.1002/lno.11136

Topp, S., Tamlin, P., Xiao, Y., Matthew, R. V. R., & Gardner, J. (2020). LimnoSat-US: A Remote Sensing Dataset for U.S. Lakes from 1984-2020 (Version 1.0.0). Zenodo. https://doi.org/10.5281/zenodo.4139695

Van der Woerd, H. J., & Wernand, M. R. (2018). Hue-Angle Product for Low to Medium Spatial Resolution Optical Satellite Sensors. *Remote Sensing*, *10*(2), 180. https://doi.org/10.3390/rs10020180

728 Vermote, E., Justice, C., Claverie, M., & Franch, B. (2016). Preliminary analysis of the performance of the Landsat 8/OLI land surface reflectance product. *Remote Sensing of Environment*, *185*, 46–56. https://doi.org/10.1016/j.rse.2016.04.008

730 Volpe, V., Silvestri, S., & Marani, M. (2011). Remote sensing retrieval of suspended sediment concentration in shallow waters. *Remote Sensing of Environment*, *115*(1), 44–54. 732 https://doi.org/10.1016/j.rse.2010.07.013

Wang, S., Li, J., Shen, Q., Zhang, B., Zhang, F., & Lu, Z. (2015). MODIS-Based radiometric 734 color extraction and classification of inland water with the forel-ule scale: A case study of lake Taihu. *IEEE Journal of Selected Topics in Applied Earth Observations and Remote* 736 *Sensing*, *8*(2), 907–918. https://doi.org/10.1109/JSTARS.2014.2360564

Wang, S., Li, J., Zhang, B., Lee, Z., Spyrakos, E., Feng, L., et al. (2020). Changes of water 738 clarity in large lakes and reservoirs across China observed from long-term MODIS. *Remote Sensing of Environment*, *247*, 111949. https://doi.org/10.1016/j.rse.2020.111949

740 Wang, W., Lee, X., Xiao, W., Liu, S., Schultz, N., Wang, Y., et al. (2018). Global lake evaporation accelerated by changes in surface energy allocation in a warmer climate. 742 *Nature Geoscience*, *11*(6), 410–414. https://doi.org/10.1038/s41561-018-0114-8

Warren Liao, T. (2005). Clustering of time series data-a survey. *Pattern Recognition*, *38*(11), 744 1857–1874. https://doi.org/10.1016/j.patcog.2005.01.025

Watson, G. S. (1964). Smooth regression analysis. *Sankhyā: The Indian Journal of Statistics,* 746 *Series A (1961-2002)*, *26*(4), 359–372.

Webster, K. E., Soranno, P. A., Cheruvelil, K. S., Bremigan, M. T., Downing, J. A., Vaux, P. D., 748 et al. (2008). An empirical evaluation of the nutrient-color paradigm for lakes. *Limnology and Oceanography*, *53*(3), 1137–1148. https://doi.org/10.4319/lo.2008.53.3.1137

750 Winder, M., & Cloern, J. E. (2010). The annual cycles of phytoplankton biomass. *Philosophical Transactions of the Royal Society B: Biological Sciences*, *365*(1555), 3215–3226. 752 https://doi.org/10.1098/rstb.2010.0125

Winder, M., & Schindler, D. E. (2004). Climate change uncouples trophic interactions in an 754 aquatic ecosystem. *Ecology*, *85*(8), 2100–2106. https://doi.org/10.1890/04-0151

Woerd, H. J. van der, & Wernand, M. R. (2015). True colour classification of natural waters with 756 medium-spectral resolution satellites: SeaWiFS, MODIS, MERIS and OLCI. *Sensors*, *15*(10), 25663–25680. https://doi.org/10.3390/s151025663

758 Woolway, R. I., & Merchant, C. J. (2019). Worldwide alteration of lake mixing regimes in response to climate change. *Nature Geoscience*, *12*(4), 271–276. 760 https://doi.org/10.1038/s41561-019-0322-x

Woolway, R. I., Kraemer, B. M., Lenters, J. D., Merchant, C. J., O'Reilly, C. M., & Sharma, S. 762 (2020). Global lake responses to climate change. *Nature Reviews Earth & Environment*, 1–16. https://doi.org/10.1038/s43017-020-0067-5

764 Xue, Z., Du, P., & Feng, L. (2014). Phenology-driven land cover classification and trend analysis based on long-term remote sensing image series. *IEEE Journal of Selected Topics in* 766 *Applied Earth Observations and Remote Sensing*, *7*(4), 1142–1156. https://doi.org/10.1109/JSTARS.2013.2294956

768 Yang, X. (2020). *Deepest point calculation for any given polygon using Google Earth Engine JavaScript API*. Zenodo. https://doi.org/10.5281/zenodo.4136755

770 Zhang, Y., & Hepner, G. F. (2017). The Dynamic-Time-Warping-based k-means++ clustering and its application in phenoregion delineation. *International Journal of Remote Sensing*, 772 *38*(6), 1720–1736. https://doi.org/10.1080/01431161.2017.1286055

Zhu, Z., Wang, S., & Woodcock, C. E. (2015). Improvement and expansion of the Fmask

774   algorithm: Cloud, cloud shadow, and snow detection for Landsats 4-7, 8, and Sentinel 2

        images. *Remote Sensing of Environment*, *159*, 269–277.

776   https://doi.org/10.1016/j.rse.2014.12.014